P. KESSLER
Department of Mechanical Engineering,
University of California at Berkeley,
Berkeley, California 94720-1740, U.S.A.
E-mail: watchwrk@me.berkeley.edu.

O. M. O'REILLY
Department of Mechanical Engineering,
University of California at Berkeley,
Berkeley, California 94720-1740, U.S.A.
Corresponding author,
Email: oreilly@me.berkeley.edu, Fax: 510-642-6163.

THE RINGING OF EULER'S DISK

Received January 23, 2002

DOI: 10.1070/RD2002v007n01ABEH000195

The motion of disks spun on tables has the well-known feature that the associated acoustic signal increases in frequency as the motion tends towards its abrupt halt. Recently, a commercial toy, known as Euler's disk, was designed to maximize the time before this abrupt ending. In this paper, we present and simulate a rigid body model for Euler's disk. Based on the nature of the contact force between the disk and the table revealed by the simulations, we conjecture a new mechanism for the abrupt halt of the disk and the increased acoustic frequency associated with the decline of the disk.

1. Introduction

The rolling circular disk is one of the most popular examples of a non-holonomically constrained rigid body. Ignoring dissipation, the equations of motion for the rolling disk were established in the late 19th century. Subsequent work by Appell [1] and Korteweg [7] showed that the equations of motion are integrable. The results of Appell and Korteweg were used nearly a century later by Cushman *et al.* [4] and O'Reilly [12] to examine, among other matters, the stability and bifurcations of the steady motions of (infinitely thin) circular disks.

The most recent toy to revive interest in the rolling disk is known as Euler's disk. This toy consists of a simple chrome-plated, cast iron cylinder. When given an an initial inclination and spin, Euler's disk starts precessing while contacting the surface. The resulting motion has two special features. First, the disk eventually comes to rest in an abrupt manner. In addition, the acoustic frequencies emitted by the disk and surface exhibit a sharp increase at the end of the motion. These two features are also exhibited by coins and many other cylindrical bodies, however Bendik *et al.* [2], the inventors of Euler's disk, optimized the choice of disk and surface so that the amount of time needed for the disk to come to rest is well over sixty seconds.

Although simulations of Euler's disk were performed by Compere [3] in the late 1990's, it was a paper by Moffatt [9] which generated considerable interest in the disk. To explain the two special features of its motion, Moffatt considered the effects of viscous dissipation on one of the types of steady motions exhibited by the disk. Moffatt's asymptotic analysis showed that the disk's motion approached a singularity in finite-time. Moffatt's paper [9] generated a substantial amount of discussion partially because several features, such as the possibility of slip and the presence of rolling friction were ignored. In particular, van den Engh *et al.* [5] and Ruina argued that sliding and rolling friction, respectively,

Mathematics Subject Classification 70E18, 70E40

were in many cases more important than viscous dissipation. To partially address these matters, McDonald and McDonald [8] considered a dissipation whose mechanical power was

$$-\epsilon mgR\left(\dot{\theta}\right)^{\beta}. \tag{1.1}$$

Here, β and ϵ are constants, and θ is one of the Euler angles used to parameterize the rotation of the disk.[1] A value of $\beta = 4$ gives agreement with Moffatt's model. Paralleling Moffatt's asymptotic analysis, but using their own experimental data, McDonald and McDonald found that a value of $\beta = 2.5$ gave good agreement with experiments. A related paper by Stanislavsky and Weron [16] extended Moffatt's analysis to incorporate the aforementioned classical integrability results for the rolling disk. These authors also attempted to correlate the frequency spectra of the undamped motions of the rolling disk to the acoustic frequencies produced by Euler's disk.

In the present paper, we choose to explore the avenues proposed by van den Engh *et al.* and Ruina. Thus, we model the disk as a rigid cylindrical body which moves with a single point of contact on a horizontal surface. The model we develop accommodates both rolling and sliding, the transition between these two idealizations, and the finite thickness of the disk. Although the model for the rolling body that we use follows Appell [1], we choose to incorporate a friction moment $\mathbf{M}_f$ as well. This moment is the primary dissipation mechanism for the rolling body, and, along with the sliding friction force, one of the dissipation mechanisms for the sliding body. In particular, our model does not incorporate Moffatt's viscous dissipation. Our model also differs from Compere's who simulated a (infinitely thin) rolling disk which was subject to a viscous dissipative moment and a dissipative force.

Because of the presence of $\mathbf{M}_f$, the model we develop is not integrable even in the rolling case. This is in contrast to the rolling case considered by Appell [1]. Furthermore, performing an analysis of the equations of motion which is similar to those performed by Cushman *et al.* [4] and O'Reilly [12] on the rolling disk does not appear to be feasible. As a result, we resort to an extensive set of numerical simulations of the model for Euler's disk. In particular, we find that the disk transitions repeatedly between rolling and sliding, that the normal force acting on the disk is always positive, and that a frequency measure of this force increases as the angle of inclination of the disk decreased. Based on the results of our numerical simulations, we conjecture, in the closing section of the paper, a new mechanism for the abrupt halt in the motion of the disk

2. Preliminaries

In this section, a rigid body model is developed for Euler's disk. We consider Euler's disk to be a rigid body of mass m which is moving on a horizontal plane (cf. figure 1). The body is assumed to have a circular cross-section of radius R and a length L, and its center of mass $\bar{X}$ is located at its geometric center. Other examples of the rigid body of interest include circular cylindrical rods and shells. The position vector of $\bar{X}$ is denoted $\bar{\mathbf{x}}$ and its velocity vector is $\bar{\mathbf{v}} = \dot{\bar{\mathbf{x}}}$. Here, a superposed dot denotes the derivative with respect to time t.

To parameterize the rotation of the rigid body, it is convenient to use a set of 3-1-2 Euler angles: θ, α, and ψ. The first two Euler angles, θ and α, can be used to define the basis $\{\mathbf{e}_1, \mathbf{e}_2, \mathbf{e}_3\}$, while the first Euler angle θ defines the basis $\{\mathbf{a}_1, \mathbf{a}_2, \mathbf{a}_3\}$:

$$\begin{bmatrix}\mathbf{a}_1\\ \mathbf{a}_2\\ \mathbf{a}_3\end{bmatrix} = \begin{bmatrix}\cos(\theta) & \sin(\theta) & 0\\ -\sin(\theta) & \cos(\theta) & 0\\ 0 & 0 & 1\end{bmatrix}\begin{bmatrix}\mathbf{E}_1\\ \mathbf{E}_2\\ \mathbf{E}_3\end{bmatrix},$$
$$\begin{bmatrix}\mathbf{e}_1\\ \mathbf{e}_2\\ \mathbf{e}_3\end{bmatrix} = \begin{bmatrix}1 & 0 & 0\\ 0 & \cos(\alpha) & \sin(\alpha)\\ 0 & -\sin(\alpha) & \cos(\alpha)\end{bmatrix}\begin{bmatrix}\mathbf{a}_1\\ \mathbf{a}_2\\ \mathbf{a}_3\end{bmatrix}. \tag{2.1}$$

[1] In Moffatt's work, the symbol Ω is used to denote $\dot{\theta} = \omega_3 \sec(\alpha)$ used in the present paper.

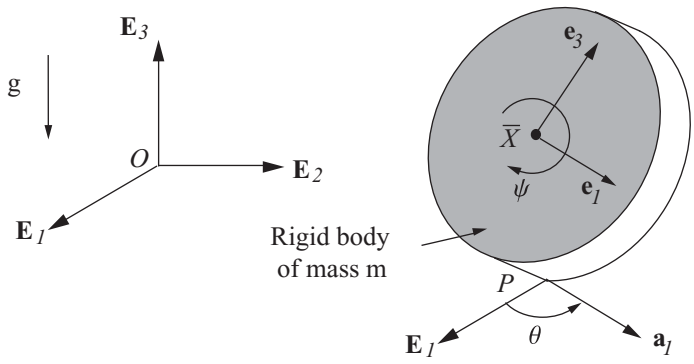

Fig. 1. A cylinder moving on a horizontal plane. This figure also illustrates two of the Euler angles used to parameterize the rigid body's rotation. The unit vector $\mathbf{e}_2 = \mathbf{e}_3 \times \mathbf{e}_1$ orients the cylinder's axis of symmetry and $\mathbf{e}_1$ is always horizontal.

Here, and in the sequel, $\{\mathbf{E}_1, \mathbf{E}_2, \mathbf{E}_3\}$ is a fixed right-handed set of Cartesian basis vectors.

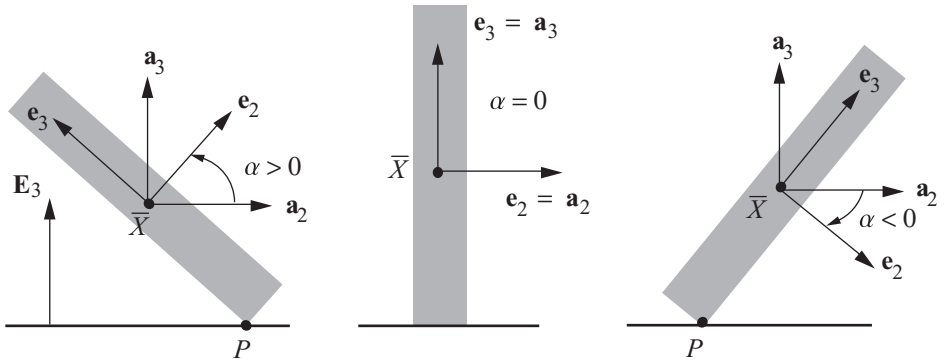

Fig. 2. Three of the contact scenarios of the rigid body with the horizontal plane. It should be noted that the vector $\mathbf{a}_3 = \mathbf{E}_3$ is normal to the horizontal plane.

The singularities of the 3-1-2 Euler angles arise when the angle of inclination $\alpha = \pm\frac{\pi}{2}$. Referring to figure 2, these singularities correspond to the body lying horizontally on the plane. This figure also illustrates how the contact between the body and the plane depends on α. When $\alpha \neq 0, \pm\frac{\pi}{2}$, there is a unique contact point P between the body and the plane. Otherwise, the contact between the body and the plane is either a line (when $\alpha = 0$) or a surface. Our interest in this paper lies in the cases where there is a single point of contact.

The angular velocity vector $\boldsymbol{\omega}$ of the body has the representations

$$\begin{aligned} \boldsymbol{\omega} &= \omega_1\mathbf{e}_1 + \omega_2\mathbf{e}_2 + \omega_3\mathbf{e}_3 = \\ &= \dot\theta\mathbf{E}_3 + \dot\alpha\mathbf{e}_1 + \dot\psi\mathbf{e}_2, \end{aligned} \tag{2.2}$$

where

$$\omega_1 = \dot\alpha, \quad \omega_2 = \dot\psi + \dot\theta\sin(\alpha), \quad \omega_3 = \dot\theta\cos(\alpha). \tag{2.3}$$

We also record the angular momentum of the body relative to its center of mass:

$$\mathbf{H} = \left(\frac{mR^2k^2}{4} + \frac{mL^2}{12}\right)(\omega_1\mathbf{e}_1 + \omega_3\mathbf{e}_3) + \left(\frac{mR^2k^2}{2}\right)\omega_2\mathbf{e}_2, \tag{2.4}$$

where $k^2 = 1$ for a solid cylindrical rod, and $k^2 = 2$ for a cylindrical shell of negligible thickness.

The instantaneous point of contact of the rigid body with the horizontal surface is denoted by P. In our model, we distinguish between two situations depending on the velocity vector $\mathbf{v}_P$ of P: the rolling case and the sliding case. Using the previous kinematical results, we can calculate a representation for $\mathbf{v}_P$:

$$\begin{aligned}\mathbf{v}_P &= \bar{\mathbf{v}} + \boldsymbol{\omega} \times (-H\mathbf{e}_2 - R\mathbf{e}_3) = \\ &= \bar{\mathbf{v}} - (R\omega_2 - H\omega_3)\mathbf{a}_1 + (R\cos(\alpha) + H\sin(\alpha))\omega_1\mathbf{a}_2 - \\ &- (H\cos(\alpha) - R\sin(\alpha))\omega_1\mathbf{E}_3. \end{aligned} \tag{2.5}$$

Here, $H = \frac{L}{2}\text{sign}(\alpha)$ and $H = 0$ when $\alpha = 0$. When the body is rolling, $\mathbf{v}_P = \mathbf{0}$. When the body is sliding, then one only has $\mathbf{v}_P \cdot \mathbf{E}_3 = 0$ and the slip velocity vector $\mathbf{v}_P$ is non-zero.

In the sliding case, it is convenient to decompose $\mathbf{v}_P$ into its components along $\mathbf{a}_1$ and $\mathbf{a}_2$:

$$\mathbf{v}_P = u_1\mathbf{a}_1 + u_2\mathbf{a}_2 = u\mathbf{s}. \tag{2.6}$$

Here, u is the slip speed and the unit vector $\mathbf{s}$ is the slip direction:

$$\mathbf{s} = \cos(\nu)\mathbf{a}_1 + \sin(\nu)\mathbf{a}_2. \tag{2.7}$$

When the slip angle ν is 0 or π, then $\mathbf{v}_P$ is parallel to $\mathbf{a}_1$. Some straightforward manipulations using (2.2), (2.5), and (2.6) show that

$$\begin{aligned}\dot{u} &= \dot{u}_1\cos(\nu) + \dot{u}_2\sin(\nu), \\ \dot{\nu} &= \frac{1}{u}\left(\dot{u}_2\cos(\nu) - \dot{u}_1\sin(\nu)\right), \\ \dot{u}_1 &= \dot{\bar{\mathbf{v}}} \cdot \mathbf{a_1} + \dot{\theta}(\mathbf{u_2} - \mathbf{R}\omega_\mathbf{1}\cos(\alpha) - \mathbf{H}\omega_\mathbf{1}\sin(\alpha)) - \mathbf{R}\dot{\omega}_\mathbf{2} + \mathbf{H}\dot{\omega}_\mathbf{3}, \\ \dot{u}_2 &= \dot{\bar{\mathbf{v}}} \cdot \mathbf{a_2} - \dot{\theta}(\mathbf{u_1} + \mathbf{R}\omega_\mathbf{2} - \mathbf{H}\omega_\mathbf{3}) + \frac{\mathbf{d^2}}{\mathbf{dt^2}}\left(\mathbf{R}\sin(\alpha) - \mathbf{H}\cos(\alpha)\right). \end{aligned} \tag{2.8}$$

The corresponding equations for the rolling body are obtained from (2.8) by setting $u_1 = u_2 = \dot{u}_1 = \dot{u}_2 = 0$.

3. Dissipation and Contact Models

We now turn to prescribing the forces and moments exerted on the body due to its contact with the horizontal surface. In most treatments of related problems involving circular disks, the contact is idealized as a single point contact, and this contact induces a force acting at the point of contact. Here, we modify this prescription by also including a moment at the idealized single point of contact. This moment, which we denote by $\mathbf{M}_f$, dissipates energy from the body both when it is rolling and sliding, and is intended to incorporate the effects of a finite region of contact in the rigid body model.

The introduction of the moment $\mathbf{M}_f$ is motivated by temporarily relaxing the assumption that the body is rigid. Such an approach has been used in the context of spheres (see, *e.g.*, Neĭmark and Fufaev [11] or Zhuravlev [17]) and in tyre models used in vehicle dynamics (see, *e.g.*, Gillespie [6] or Pacejka [13]). Briefly, because any body is deformable, the actual contact between the body and the horizontal surface will involve a contact region $\mathcal{A}$ rather than a single point. The body will be subject to a traction field $\mathbf{t}$ over this region. Determining $\mathbf{t}$ and $\mathcal{A}$, especially for the dynamic problem of interest in this paper, is presently intractible. Within the context of rigid body dynamics, the traction field is equipollent to the sum of a normal force $\mathbf{N}$ and a friction force $\mathbf{F}_f$ acting at P and a moment $\mathbf{M}_f$. That is, the moment $\mathbf{M}_f$ represents the resultant moment of the field $\mathbf{t}$ at P. We shall use standard prescriptions for $\mathbf{N}$ and $\mathbf{F}_f$ and propose a new prescription for $\mathbf{M}_f$.

The normal force acting on the body at P has the representation $\mathbf{N} = N\mathbf{E}_3$. When the body is rolling, we assume that the friction force $\mathbf{F}_f$ has the representation

$$\mathbf{F}_f = F_{f1}\mathbf{a}_1 + F_{f2}\mathbf{a}_2, \tag{3.1}$$

where F_{f1} and F_{f2} are determined from the balance laws. The force $\mathbf{F}_f$ is subject to the static friction criterion: $\sqrt{F_{f1}^2 + F_{f2}^2} \leqslant \mu_s|N|$, where μ_s is the constant coefficient of static Coulomb friction. When the body is sliding, we assume that the friction force $\mathbf{F}_f$ is

$$\mathbf{F}_f = -\mu_d|N|\frac{u_1\mathbf{a}_1 + u_2\mathbf{a}_2}{\sqrt{u_1^2 + u_2^2}} = -\mu_d|N|\mathbf{s}, \tag{3.2}$$

where $\mu_d \geqslant 0$ is the (constant) coefficient of dynamic friction.

For the moment $\mathbf{M}_f$, we parallel the prescription (3.2):

$$\mathbf{M}_f = -\sum_{i=1}^{3} k_i|N|\left(\operatorname{sign}(\boldsymbol{\omega}\cdot\mathbf{a}_i)\right)\mathbf{a}_i, \tag{3.3}$$

where $k_1 \geqslant 0$, $k_2 \geqslant 0$, and $k_3 \geqslant 0$ are constants. It is not too difficult to see that k_1, k_2, and k_3 will depend on the dimensions of the contact region $\mathcal{A}$. To motivate our choice of the components $\boldsymbol{\omega}\cdot\mathbf{a}_i$ in (3.3), observe that $\mathbf{a}_1$ and $\mathbf{a}_2$ are tangent to the horizontal plane contacting the body, while $\mathbf{a}_3 = \mathbf{E}_3$ is normal to this plane. Because $\mathcal{A}$ is oriented by $\mathbf{a}_1$ and $\mathbf{a}_2$, the choice of these components as opposed to $\boldsymbol{\omega}\cdot\mathbf{e}_i$, for instance, seems more appropriate. Finally, the assumption that k_1, k_2, and k_3 are non-negative is motivated by the requirement that $\mathbf{M}_f$ dissipates energy from the disk, *i.e.*, $\mathbf{M}_f\cdot\boldsymbol{\omega} \leqslant 0$. This requirement can also be interpreted as $\mathbf{M}_f$ opposing the rotation of the rigid body.

The five constants, k_1, k_2, k_3, μ_s, and μ_d, associated with $\mathbf{F}_f$ and $\mathbf{M}_f$ must be experimentally determined. We also note that the prescription for $\mathbf{M}_f$ is not unique. Indeed several others are discussed in the literature (see, *e.g.*, [11, 17]). One could, for instance, also assume that $\mathbf{M}_f$ depended on $\mathbf{F}_f$. However, we are of the opinion that (3.3) provides a tractible, yet physically realistic model.

4. Equations of Motion for the Sliding Body

The equations of motion for the sliding body can be obtained using a balance of linear momentum,

$$-mg\mathbf{E}_3 + \mathbf{N} + \mathbf{F}_f = m\dot{\mathbf{v}}, \tag{4.1}$$

and a balance of angular momentum,

$$(-R\mathbf{e}_3 - H\mathbf{e}_2)\times(\mathbf{N} + \mathbf{F}_f) + \mathbf{M}_f = \dot{\mathbf{H}}. \tag{4.2}$$

In these equations, $\mathbf{F}_f$ and $\mathbf{M}_f$ are prescribed by (3.2) and (3.3), respectively.

When supplemented by the sliding condition $\mathbf{v}_P\cdot\mathbf{E}_3 = 0$, (4.1) and (4.2) constitute seven equations to determine the unknown normal force $\mathbf{N}$ and the motion of the body. Indeed, it is easy to see from (4.1) that

$$\mathbf{N} = N\mathbf{E}_3 = m\left(g + \frac{d^2}{dt^2}\left(H\sin(\alpha) + R\cos(\alpha)\right)\right)\mathbf{E}_3. \tag{4.3}$$

Rather than solving directly for the motion of the center of mass and the orientation of the disk, it is convenient to first establish the differential equations governing the slip speeds, u_1 and u_2, along with the angular speeds, ω_1, ω_2, and ω_3, and the angle of inclination α. These equations are obtained from (4.1) and (4.2) with the assistance of (2.8). The solutions of these equations can then be used to determine the position of the center of mass $\bar{\mathbf{x}}$ and the Euler angles $\theta(t)$, $\alpha(t)$, and $\psi(t)$. Prior

to recording these equations, we introduce the following aspect ratio, dimensionless velocities, and dimensionless time:

$$h = \frac{H}{R}, \quad \widehat{u}_\beta = \left(\frac{\chi}{R}\right) u_\beta, \quad \widehat{\omega}_i = \chi\omega_i, \quad \tau = \frac{t}{\chi}, \tag{4.4}$$

where

$$\chi = \sqrt{\left(\frac{k^2+4}{4}\right)\frac{R}{g}}. \tag{4.5}$$

In addition, the dimensionless normal force component is, from (4.3),

$$\Phi = \left(\frac{\chi^2}{mR}\right) N = \frac{k^2+4}{4} + \frac{d^2}{d\tau^2}\left(\cos(\alpha) + h\sin(\alpha)\right). \tag{4.6}$$

As it is necessary for contact of the disk and the horizontal plane, we shall assume that Φ is strictly positive.

The differential equations of interest are

$$\begin{aligned}
\frac{du_1}{d\tau} + \frac{d\omega_2}{d\tau} - h\frac{d\omega_3}{d\tau} &= \omega_3\sec(\alpha)(u_2 - \omega_1 e) - \mu_d\Phi\cos(\nu),\\
\frac{du_2}{d\tau} - e\frac{d\omega_1}{d\tau} &= -\omega_3\sec(\alpha)(u_1 + \omega_2 - h\omega_3) + f\omega_1^2 - \mu_d\Phi\sin(\nu),\\
\frac{d\alpha}{d\tau} &= \omega_1,\\
\left(1 + \frac{4h^2}{3k^2} + \frac{4f^2}{k^2}\right)\frac{d\omega_1}{d\tau} &= \omega_3\left(2\omega_2 - \left(1 + \frac{4h^2}{3k^2}\right)\omega_3\tan(\alpha)\right) -\\
&\quad - f\left(1 + \frac{4}{k^2}\right) + \left(\frac{4ef}{k^2}\right)\omega_1^2 -\\
&\quad - \left(\frac{4\mu_d e}{k^2}\right)\Phi\sin(\nu) - \left(\frac{4k_1}{k^2R}\right)\Phi\mathrm{sign}(\omega_1),\\
\frac{d\omega_2}{d\tau} &= \left(\frac{2\mu_d}{k^2}\right)\Phi\cos(\nu) - \left(\frac{2\bar{k}_2}{k^2R}\right)\Phi,\\
\left(1 + \frac{4h^2}{3k^2}\right)\frac{d\omega_3}{d\tau} &= -\omega_1\left(2\omega_2 - \left(1 + \frac{4h^2}{3k^2}\right)\omega_3\tan(\alpha)\right) -\\
&\quad - \left(\frac{4\mu_d h}{k^2}\right)\Phi\cos(\nu) - \left(\frac{4\bar{k}_3}{k^2R}\right)\Phi.
\end{aligned} \tag{4.7}$$

Here, for convenience, we have defined

$$\begin{aligned}
\bar{k}_2 &= k_2\cos(\alpha)\mathrm{sign}(\boldsymbol{\omega}\cdot\mathbf{a}_2) + k_3\sin(\alpha)\mathrm{sign}(\boldsymbol{\omega}\cdot\mathbf{a}_3),\\
\bar{k}_3 &= k_3\cos(\alpha)\mathrm{sign}(\boldsymbol{\omega}\cdot\mathbf{a}_3) - k_2\sin(\alpha)\mathrm{sign}(\boldsymbol{\omega}\cdot\mathbf{a}_2),
\end{aligned} \tag{4.8}$$

and

$$e = h\sin(\alpha) + \cos(\alpha), \quad f = \frac{de}{d\alpha} = h\cos(\alpha) - \sin(\alpha). \tag{4.9}$$

In (4.7), we have dropped the hats ornamenting the dimensionless variables.

Equations $(4.7)_{1,2}$ were obtained from (2.8) where $\dot{\tilde{\mathbf{v}}}\cdot\mathbf{a}_\alpha$ was specified using the $\mathbf{a}_\alpha$ component of (4.1). The remaining four differential equations $(4.7)_{3,4,5,6}$ were obtained using (2.2) and the $\mathbf{e}_i$ components of (4.2). In order to illuminate the dissipative terms in (4.7), we refrained from substituting for Φ using (4.6). However, prior to numerically integrating (4.7), we do perform this substitution.

5. Equations of Motion for the Rolling Body

When the body is rolling, the constraint $\mathbf{v}_P = \mathbf{0}$ and the equation (2.8) can be used to calculate the acceleration of the center of mass in terms of the rotational kinematics of the body:

$$\begin{aligned}\dot{\bar{\mathbf{v}}} \cdot \mathbf{a_1} &= \dot{\theta}(R\omega_1 \cos(\alpha) + H\omega_1 \sin(\alpha)) + R\dot{\omega}_2 - H\dot{\omega}_3,\\ \dot{\bar{\mathbf{v}}} \cdot \mathbf{a_2} &= \dot{\theta}(R\omega_2 - H\omega_3) + \frac{d}{dt}\left((R\cos(\alpha) + H\sin(\alpha))\omega_1\right).\end{aligned} \tag{5.1}$$

Following Routh (1905), we can use (5.1) along with a balance of linear momentum of the form (4.1), to calculate expressions for the forces $\mathbf{N}$ and $\mathbf{F}_f$ as functions of the rotational kinematics. Omitting details, the dimensionless form of these forces is

$$\begin{aligned}\widehat{\mathbf{F}}_f = \left(\frac{\chi^2}{mR}\right)\mathbf{F}_f &= \left(\frac{d\omega_2}{d\tau} - h\frac{d\omega_3}{d\tau} + e\omega_1\omega_3\sec(\alpha)\right)\mathbf{a}_1 + \\ &+ \left(-e\frac{d\omega_1}{d\tau} - f\omega_1^2 + (\omega_2 - h\omega_3)\,\omega_3\sec(\alpha)\right)\mathbf{a}_2,\\ \Phi\mathbf{E}_3 &= \left(\frac{k^2+4}{4} + \frac{d^2e}{d\tau^2}\right)\mathbf{E}_3.\end{aligned} \tag{5.2}$$

It should be noted that $(5.2)_2$ is, as expected, identical to (4.6), and that we have omitted the hats ornamenting the dimensionless speeds in (5.2).

The balance of angular momentum of the rolling body is used in conjunction with (5.2) to determine the differential equations governing the rotation of the rolling body. Omitting details, and non-dimensionalizing the resulting equations, we find the following four first-order differential equations:

$$\begin{aligned}\frac{d\alpha}{d\tau} &= \omega_1,\\ \left(1 + \frac{4}{k^2} + \frac{16h^2}{3k^2}\right)\frac{d\omega_1}{d\tau} &= \omega_3\left(2\omega_2 - \left(1 + \frac{4h^2}{3k^2}\right)\omega_3\tan(\alpha)\right) + \\ &+ \left(\frac{4e}{k^2}\right)\omega_3\sec(\alpha)\,(\omega_2 - h\omega_3) - \\ &- f\left(1 + \frac{4}{k^2}\right) - \left(\frac{4k_1}{k^2R}\right)\Phi,\\ \frac{d\omega_2}{d\tau} - \left(\frac{2h}{k^2+2}\right)\frac{d\omega_3}{d\tau} &= -\left(\frac{2e}{k^2+2}\right)\omega_1\omega_3\sec(\alpha) - \\ &- \left(\frac{2\bar{k}_2}{(k^2+2)R}\right)\Phi,\\ \left(1 + \frac{16h^2}{3k^2}\right)\frac{d\omega_3}{d\tau} - \left(\frac{4h}{k^2}\right)\frac{d\omega_2}{d\tau} &= -\omega_1\left(2\omega_2 - \left(1 + \frac{4h^2}{3k^2}\right)\omega_3\tan(\alpha)\right) + \\ &+ \left(\frac{4he}{k^2}\right)\omega_1\omega_3\sec(\alpha) - \left(\frac{4\bar{k}_3}{k^2R}\right)\Phi.\end{aligned} \tag{5.3}$$

As in the sliding case, we have not yet substituted for Φ using $(5.2)_2$ in (5.3), and we have dropped the hats ornamenting the dimensionless variables. However, prior to numerically integrating (5.3), we do perform this substitution.

The solutions, $\hat{\omega}_i(\tau)$ and $\alpha(\tau)$, of (5.3) can be substituted into (5.2) to determine $\mathbf{F}_f$ and $\mathbf{N}$ as functions of time. They can also be used to determine the orientation of the body as a function of time, and, using the rolling condition $\mathbf{v}_P = \mathbf{0}$, they can be used to determine $\bar{\mathbf{x}}(t)$.

6. Comments on the Governing Equations

6.1. Integrability

In seminal works, Appell [1] and Korteweg [7] showed that the equations of motion for the rolling disk (with $\mathbf{M}_f = 0$) could be integrated analytically to provide $\alpha(t)$ and $\omega_i(t)$.[2] Appell [1] indicated how the equations of motion for the rolling cylindrical body discussed in the present paper also had this feature. The method by which he showed these results can be extended to the equations governing the sliding body discussed in this paper provided $\mathbf{M}_f = \mathbf{0}$ and $\mu_d = 0$.

When $\mathbf{M}_f \neq \mathbf{0}$ for the rolling cylindrical body and when $\mathbf{M}_f \neq \mathbf{0}$ or $\mu_d \neq 0$ for the sliding cylindrical body, the techniques used by Appell and Korteweg no longer apply. Indeed, we were unable to show that either (4.7) or (5.3) were integrable in this cases. Consequently, we resorted to numerical simulations of the governing equations of the rigid body.

6.2. Transitions from and to rolling

For the simulations to be presented, we prescribe a set of initial conditions for the rigid body: $\bar{\mathbf{v}}(t_0)$, $\boldsymbol{\omega}(t_0)$ and $\alpha(t_0)$. The resulting velocity of P is examined to ascertain whether or not the body is slipping or rolling. Depending on $\mathbf{v}_P$, either (5.3) in the rolling case, or (4.7) in the sliding case are integrated. At each stage of the integration of (5.3), the static friction criterion is examined to verify that sufficient static friction is present for the body to roll. If this criterion is violated, then the body has started to slip and the use of (4.7) is initiated. The initial slip direction $\mathbf{s}$ (or, equivalently, the angle ν) is determined by examining the direction of $\mathbf{F}_f$ (cf. (5.2)) at the instant prior to the violation of the static friction criterion, and the initial slip speed u is set to a small prescribed value. During the numerical integration of (4.7), the slip speed is continually monitored. In the event that the magnitude of the slip speed becomes lower than a prescribed tolerance, the body is assumed to be rolling and the numerical integration proceeds with (5.3).

6.3. Energetic considerations

The dimensionless total energy $\tilde{E}$ of the body is

$$\tilde{E} = \left(\frac{\chi^2}{mR^2}\right) E = \frac{1}{2}\left(u_1 + \omega_2 - h\omega_3\right)^2 + \frac{1}{2}\left(u_2 + e\omega_1\right)^2 + \\ + \frac{1}{2}\left(\frac{k^2}{4} + \frac{h^2}{3}\right)\left(\omega_1^2 + \omega_3^2\right) + \left(\frac{k^2}{4}\right)\omega_2^2 + \\ + \left(\frac{k^2+4}{4}\right)(e-h)\,. \tag{6.1}$$

Again, we have omitted the hats ornamenting the dimensionless speeds in this equation. When $\mathbf{M}_f = \mathbf{0}$ and $\mu_d > 0$, it is easy to prove that E of the rolling rigid body must be conserved while it decreases monotonically for the sliding body. In addition, for the rolling rigid body, when $\mathbf{M}_f \neq \mathbf{0}$, then E decreases monotically. As a check on the numerical simulations, the aforementioned behavior of the total energy was verified.

7. Simulations

For the simulations, we use the dimensions of Tangent Toy's Euler's disk:

$$k = 1, \quad R = 3.755\text{cm}, \quad L = 1.28\text{cm}, \quad m = 0.4387\text{kg}. \tag{7.1}$$

[2] Further details on, and extensions to, Appell and Korteweg's work can be found in [4, 12].

Consequently,

$$h = \frac{7.51}{1.28}, \quad \chi = 0.0691712. \tag{7.2}$$

It is important to note that an interval of τ corresponding to 100 is equivalent to a time interval of 6.91712 seconds.

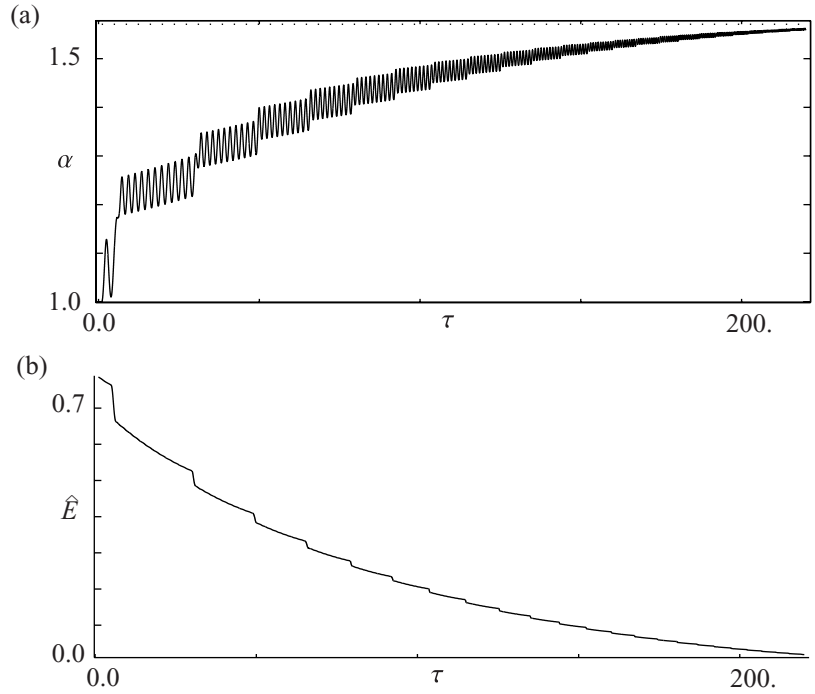

Fig. 3. (a) The variation of the angle α (radians) with dimensionless time τ. (b) The decline of the dimensionless total energy $\hat{E}$ of the disk.

For the simulations whose results are presented in figures 3–6, the following set of friction coefficients were used:

$$\mu_s = 0.5, \quad \mu_k = 0.3, \quad \frac{k_1}{R} = 0.0001, \quad \frac{k_2}{R} = 0.0008, \quad \frac{k_3}{R} = 0.008. \tag{7.3}$$

These values can be considered representative, and probably differ from the values for Tangent Toy's Euler's disk.

A representative set of initial conditions for Euler's disk arises when it is inclined to the horizontal plane and given an initial angular velocity about $\mathbf{e}_3$. With this scenario in mind, we use the following set of initial conditions in the simulations we present:

$$\begin{gathered} \bar{\mathbf{x}}(t=0) = \mathbf{0}, \;\; \mathbf{v}_P(t=0) = \mathbf{0}, \; \hat{\boldsymbol{\omega}}(t=0) = -\mathbf{e}_3, \\ \alpha(t=0) = 1.0, \; \theta(t=0) = 0.0, \;\; \phi(t=0) = 0.0. \end{gathered} \tag{7.4}$$

Referring to figure 3, we see that the angle α tends to $\frac{\pi}{2}$ as time increases for this simulation. Correspondingly, the total energy of the disk decreases. The slope of the $\hat{E}$ versus τ graph can be used to ascertain whether the disk is rolling or sliding. Specifically, during sliding the dissipation of energy is larger than it is during rolling.

We note that the model we have developed for Euler's disk does not appear to possess a finite-time singularity. By allowing the simulations to run for a sufficiently large period of time, we are able to

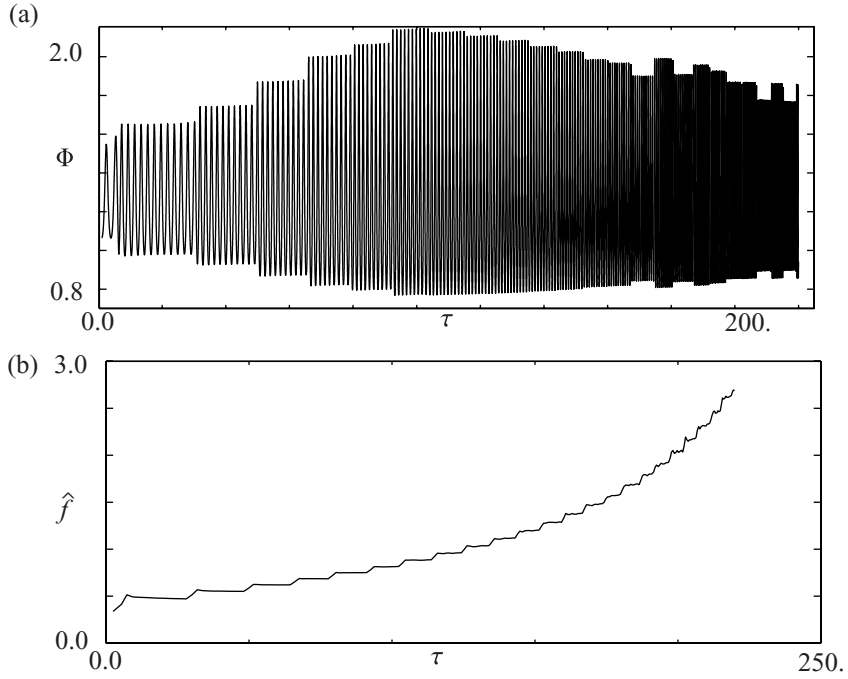

Fig. 4. (a) The variation of the dimensionless normal force Φ with dimensionless time τ. (b) The "frequency" $\hat{f}$ of the normal force as a function of the dimensionless time τ. For Tangent Toy's Euler's disk, a value of $\hat{f} = 2.5$ corresponds to a frequency of 36 Hz.

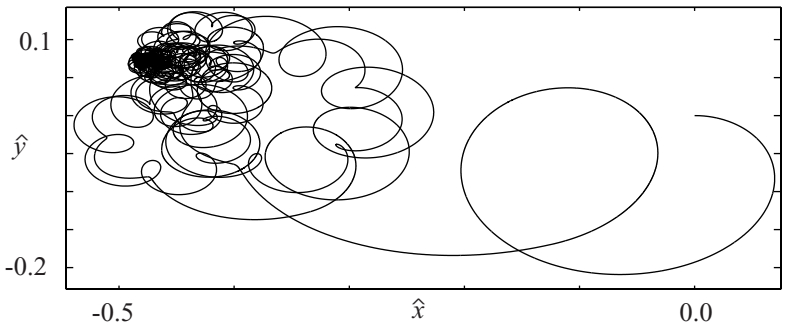

Fig. 5. The path of the center of mass of the disk. In this figure, $\hat{x} = (\bar{\mathbf{x}} \cdot \mathbf{E}_1)/R$ and $\hat{y} = (\bar{\mathbf{x}} \cdot \mathbf{E}_2)/R$.

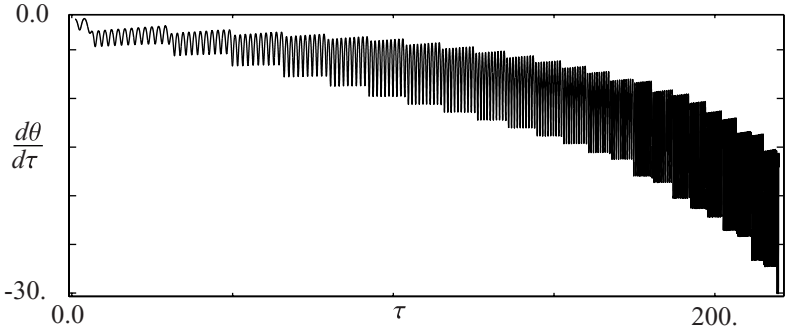

Fig. 6. The angular rate $\dfrac{d\theta}{d\tau} = \hat{\omega}_3 \sec(\alpha)$ as a function of the dimensionless time τ.

attain final values of α which are, subject to machine precision, arbitrarily close to $\frac{\pi}{2}$. From several other sets of simulations, we find that the time taken for α to achieve a value arbitrarily close to $\frac{\pi}{2}$ depends on the value of the parameters μ_d, k_1, k_2, and k_3 (cf. (7.3). Indeed, by increasing the value of these parameters we can decrease this time.

The normal force Φ acting on the disk has an unusual temporal behavior. As shown in figure 4, a frequency $\hat{f}$ associated with this force increases as the angle of inclination of the disk tends to zero.[3] The corresponding figure for the angular speed $\frac{d\theta}{d\tau}$ was for the most part identical. The increase in $\hat{f}$ observed in figure 4(b) is qualitatively (but not quantitatively) similar to the results for $\frac{d\theta}{d\tau}$ that are presented in McDonald and McDonald [8]. It should be clear from figure 4(a) that the spectral content of $\Phi(\tau)$ is considerable. Another interesting feature of the normal force is that it is never zero. In other words, the disk does not loose contact with the surface.

The behavior of the center of mass as the disk's angle of inclination $\frac{\pi}{2} - \alpha$ decreases is also of interest. For the representative initial conditions and parameters chosen, figure 5 shows the in-plane components of $\hat{\mathbf{x}}(\tau)$. Notice that as the angle of inclination decreases, the in-plane motion of the center of mass of the disk diminishes considerably until it is almost negligible. Finally, we also wish to point out that the results shown in figure 6 illustrate that $\frac{d\theta}{d\tau}$ grows considerably as the disk becomes horizontal. Both the behavior of the center of mass and that of the angular rate $\frac{d\theta}{d\tau}$ have been noted by others for the actual Euler disk. Indeed, they are invoked by Moffatt [9] in his analysis of Euler's disk.

8. Concluding Comments and a Conjecture

There are two interesting features of Euler's disk that have attracted considerable attention. The first of these is the increase in the audible frequency that the disk produces as it declines, and the second is the abrupt halting of its motion. Our model shows that the frequency of the motion increases as the disk declines. This however is not the primary sound source of the system. To produce sound, the actual disk and the surface that it moves on vibrates. Because we are using rigid body models for both of these objects, we cannot capture this vibration. However, we believe that the normal force behavior that we report can be considered as a measure of the forcing experienced by the actual disk and surface. This forcing will excite modes of vibration of the disk and consequently produce sound. Indeed, an examination of the modes of vibration of Tangent Toys' Euler's disk using a finite element model shows that it has at least four modes of vibration in the audible range of humans.[4] As the disk continues its decline, we conjecture that the vibrations of the disk and surface will eventually result in it losing contact with the surface. When this occurs, the angle of inclination of the disk is small and so the ensuing impact of the disk and surface constitutes the abrupt end of the disk's motion.

To prove our conjecture, it will be necessary to use a deformable model for both the disk and the table. Although the finite element method is a viable approach to developing this model, the ensuing computations will be very expensive.

[3]The frequency $\hat{f}$ was calculated from $\Phi(\tau)$ by determining the time T between three successive peaks and setting $\hat{f} = 2/T$.

[4]We are grateful to Nathan Kinkaid for these finite element calculations. He considered the disk to be isotropically elastic with a Young's modulus of 195 GPa, a density of 7737.27 kg/m^2, and a Poisson's ratio of 0.28. To approximate the contact condition, several neighboring points on the lateral surface of the disk were fixed.

Acknowledgements

O'Reilly's work was partially supported by grant number CMS-0084808 from the U. S. National Science Foundation. Kessler's work was partially supported by a GAANN Award from the U. S. Department of Education. Both authors gratefully acknowledge this support.

References

[1] *P. Appell.* Sur l'intégration des équations du mouvement d'un corps pesant de révolution roulant par une arête circulaire sur un plan horizontal; cas particulier du cerceau. Rend. Circ. Mat. Palermo. V. 14. 1900. P. 1–6.

[2] *J. J. Bendik, Jr., L. J. Shaw, R. H. Wyles.* Spinning/rolling disc. U. S. Patent No. 5863235, 1999.

[3] *M. Compere.* http://marc.me.utexas.edu/animation.

[4] *R. Cushman, J. Hermans, D. Kemppainen.* The rolling disc. In H. W. Broer, S. A. van Gils, I. Hoveijn and F. Takens, editors. Progr. Nonlinear Differential Equations Appl. V. 19. 1996. P. 21–60.

[5] *G. van den Engh, P. Nelson, J. Roach.* Numismatic gyrations. Nature. V. 408. 2000. P. 540.

[6] *T. D. Gillespie.* Fundamentals of Vehicle Dynamics. Warrendale, Pennsylvania, Society of Automotive Engineers. 1992.

[7] *D. J. Korteweg.* Extrait d'une lettre à M. Appell. Rend. Circ. Mat. Palermo. V. 14. 1900. P. 7–8.

[8] *A. J. McDonald, K. T. McDonald.* The rolling motion of a disk on a horizontal plane. Preprint Archive, Los Alamos National Laboratory. arXiv: physics/008227. 2000.

[9] *H. K. Moffatt.* Euler's disk and its finite-time singularity. Nature. V. 404. 2000. P. 833–834.

[10] *H. K. Moffatt.* Reply to "Numismatic gyrations". Nature. V. 408. 2000. P. 540.

[11] *Ju. I. Neĭmark, N. A. Fufaev.* Dynamics of Nonholonomic Systems. Providence, American Mathematical Society. 1972.

[12] *O. M. O'Reilly.* The dynamics of rolling disks and sliding disks. Nonlinear Dynam. V. 10. 1996. P. 287–305.

[13] *H. B. Pacejka.* Modelling of tyre force and moment generation. In B. Jacobson and J. J. Kalker, editors. Rolling Contact Phenomena. P. 277–327. Vienna and New York, Springer–Verlag. 2000.

[14] *E. J. Routh.* The Advanced Part of a Treatise on the Dynamics of a System of Rigid Bodies. 6th ed. London, Macmillan. 1905.

[15] *A. Ruina.* Comments on "Euler's disk and its finite–time singularity" by H. K. Moffatt. Unpublished notes. Department of Theoretical and Applied Mechanics, Cornell University. 2000.

[16] *A. A. Stanislavsky, K. Weron.* Nonlinear oscillations in the rolling motion of Euler's disk. Physica D. V. 156. 2001. P. 247–259.

[17] *V. G. Zhuravlev.* The model of dry friction in the problem of the rolling of rigid bodies. J. Appl. Math. Mech. V. 62. 1998. P. 705–710.